JOURNAL OF MATERIALS SCIENCE 19 (1984) 385–395

Fatigue-crack advance mechanisms in polymers

Part 2 *Semicrystalline polymers for $T<T_g$ (polybutylene terephthalate)*

T. A. MORELLI, M. T. TAKEMORI
Polymer Physics and Engineering Branch, Corporate Research and Development, General Electric Company, Schenectady, New York 12301, USA

The room-temperature fatigue-crack propagation behaviour of poly(butylene terephthalate) is strongly influenced by hysteretic heating near the crack tip since the glass transition temperature is just above room temperature. At low frequencies or stress intensities, the crack tip damage zone consists of several layers of crazes. At high frequencies or stress intensities, hysteretic heating causes a drop in yield stress and a large increase in the depth of the crack tip damage layer. At the same time, the increase in the plane stress plastic zones near the free surfaces produces large shear lips which flank the interior craze zone. This transformation results in a crack growth rate transition which appears as a crack deceleration followed by rapid crack acceleration. This thermal transition can be suppressed or delayed by immersion in water or silicone oil to reduce heat build-up in the sample during testing.

1. Introduction

The fatigue crack propagation (FCP) behaviour of semicrystalline polymers is strongly dependent on the glass transition temperature (T_g). For a polymer tested above its T_g the crack tip is often preceeded by a large halo of crazes which initiate in the interspherulitic boundaries and the interlamellar regions [1, 2]. The formation of this extended damage zone is due to the low yield stresses of semicrystalline polymers above their T_gs. Polymers tested below their T_gs, however, often possess a much smaller crack tip craze cluster. For these polymers hysteretic heating can sometimes lead to large temperature rises with dramatic changes in the crack growth behaviour. This latter class of semicrystalline polymers ($T<T_g$) will be discussed in this paper, using poly(butylene terephthalate) (PBT) as an example, while the former case ($T>T_g$) will be the subject of a future paper.

The need to characterize the damage processes occurring in the fatigue crack tip damage zone has been demonstrated by several recent experimental observations on polyvinylidene fluoride (PVDF) [1], polycarbonate [3] and blends of poly(2,6-dimethyl-1,4-phenylene oxide) and polystyrene [4]. In these studies, fatigue cracks were observed to propagate through extensive damage layers consisting of sheared regions and/or crazes. Since most of the energy dissipation occurred in these crack layers rather than in the formation of the crack surfaces, a knowledge of the mechanisms of damage layer formation would be required for an understanding of the FCP behaviour. A theoretical model, the crack layer model, has been recently developed by Chudnovsky and Moet [5] to provide a quantitative description of the FCP process. Our present work is intended to describe the mechanisms of damage dissemination at the crack tip and will not attempt to quantitatively assess the crack growth behaviour.

Prior studies on the fatigue behaviour of semicrystalline polymers has not been extensive. Earlier work in the late 1960s and early 1970s focused on the thermal runaway failure of un-

0022–2461/84 $03.00 + .12

notched nylon, poly(ethylene) (PE) and poly(tetrafluoroethylene) (PTFE) [6, 7]. Later studies focused on the effects of microstructural differences produced by varying processing conditions [8], on the relationship between thermal softening and fatigue crack development [9–11] and on the stress concentrating effects of holes and weld lines [8, 12, 13].

More recently, the FCP behaviour of semicrystalline polymers, such as low- and high-density PE, PVDF, nylon, poly(acetal) and poly(propylene) (PP) have been reported [1, 2, 14–21]. With the notable exception of a recent paper by Bretz *et al.* [1], few studies have investigated the microdamage mechanisms preceeding the fatigue crack tip. In that paper it was concluded that the compressive stresses in the fully reversed crack tip plastic zone led to the elongation of spherulites along the crack propagation direction, as well as the crushing or flattening of these elongated spherulites in PVDF.

Sandt and Hornbogen [15] observed a region of crack growth arrest, where cracks initiated from a sharp razor slice decelerated and appeared to arrest in PP, PTFE and poly(butylene). This curious behaviour was ascribed to the high reversible strains in these polymers and their helical molecular structures.

Andrews and Walker [16] reported two regions of FCP behaviour in low-density PE – a brittle-like and a ductile-like region, which were linked by a transition region. No reasons for this transition were given and a plane strain to plane stress transition was not believed to be responsible. Bretz *et al.* [18] later reported a similar discontinuity and reported fracture surface observations which indicated a change from small voids to large voids in the two regions.

2. Experimental procedure

FCP testing was performed on an Instron 1350 servohydraulic test system under sinusoidal loading in tension–tension with a minimum to maximum load ratio of 0.1. Because of the length of the tests (some lasted over 200 h), video recordings were made on an NEC VC-9507 time-lapse video cassette recorder. The crack lengths were measured during subsequent playback of the video recordings.

Compact tension specimens were machined from 0.635 cm thick injection-moulded bars of PBT (General Electric Co. Valox® Thermoplastic polyester, Grade 310). The stress intensity factor is given by [22]:

$$K_I = \frac{P}{BW^{1/2}} \frac{2+x}{(1-x)^{3/2}} (0.886 + 4.64x - 13.32x^2 + 14.72x^3 - 5.6x^4)$$

where P is the applied load, B is the specimen thickness, W is the distance from the pin loading axis to the back edge of the specimen, and $x = l/W$, with l the crack length.

In all cases the starter crack was grown under cyclic loading from a razor cut made in the initial saw cut. Crack growth data were recorded only after the crack had grown a few mm beyond the initial razor cut.

The surface temperature near the crack tip was monitored in a few samples with a nickel resistance thermometer, which was positioned a few millimetres ahead and to one side of the crack tip.

The fracture surfaces were examined with a Toho Instruments Super II scanning electron microscope. The fracture surface profiles and the subsurface regions were studied by transmission light microscopy with a Zeiss microscope. For the subsurface studies, thin sections (approximately 25 to 50 μm thick) were prepared by standard metallographic grinding and polishing techniques. Both transverse and longitudinal sections were prepared.

3. Static tensile measurements

Static tensile properties were measured on the servohydraulic testing machine at a stroke rate of 0.25 cm sec^{-1}. Tests were performed on tensile bars machined from the same injection-moulded plaques used for the fatigue tests at 24, 50 and 80° C. Relative results are tabulated in Table I. Since the T_g of PBT is roughly 50° C, large variations can be seen in these values at the three different temperatures.

4. FCP results

The FCP response of PBT shows several distinct regions of crack growth behaviour, as schematically

TABLE I Relative properties

Temperature (°C)	Yield stress	Modulus	Strain at break
24	1	1	1
50	0.70	0.40	2.0
80	0.45	0.20	2.6

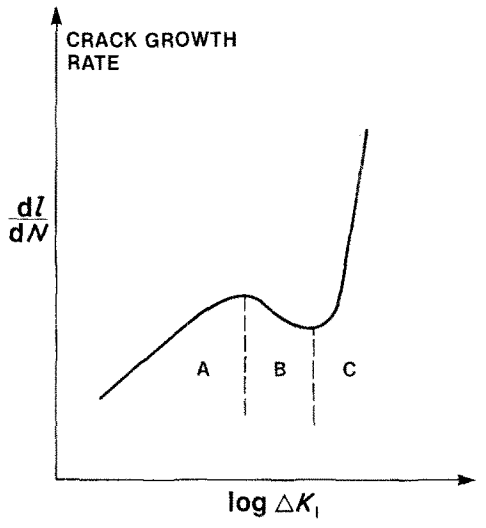

Figure 1 Schematic drawing of FCP behaviour showing transition. See text for explanation.

illustrated in Fig. 1. At low stress intensity ranges (A) the crack growth rates are slow and frequency independent with no significant bulk heating. A transition, which is characterized by a deceleration in the crack growth rate and a gradual rise in the temperature near the crack front, occurs at higher ΔK_I levels (B). This transition is a strong function of test frequency and is very pronounced in the high frequency tests. At even higher ΔK_I levels (C) thermal runaway takes place, i.e. a large portion of the specimen near the crack tip heats up (exceeding the T_g of PBT) and the crack growth rate accelerates rapidly.

Results of tests run between 0.01 and 20 Hz are shown in Fig. 2 where the different FCP zones can be seen. At the high frequencies (> 4 Hz) the transition zone is broad with a noticeable crack deceleration, whereas at the low frequencies, its existence is less clear. Fracture surface observations, to be described later, must be used to corroborate their presence.

The free surface temperature near the crack tip for a 4 Hz test is depicted in Fig. 3, which reveals a gradual temperature rise during the transition zone and a very rapid increase in the post-transition region. This reflects large scale bulk heating.

Since the onset of the thermal transition is related to the rate of hysteretic heat generation, a strong dependency on test frequency is expected. This dependency is illustrated in Fig. 4, which shows ΔK_I^* (the value of ΔK_I at the onset of the thermal transition, i.e. at the beginning of crack growth deceleration) plotted against test frequency. Rapid heat accumulation at the high frequencies (> 10 Hz) leads to low values of ΔK_I^* (1.6 to 3.5 MN m$^{-3/2}$) whereas at lower frequencies the thermal transition is delayed to higher ΔK_I^* values.

A strong frequency dependence is also evident for the occurrence of thermal runaway. As the frequency drops from 20 Hz to 0.1 Hz, the onset

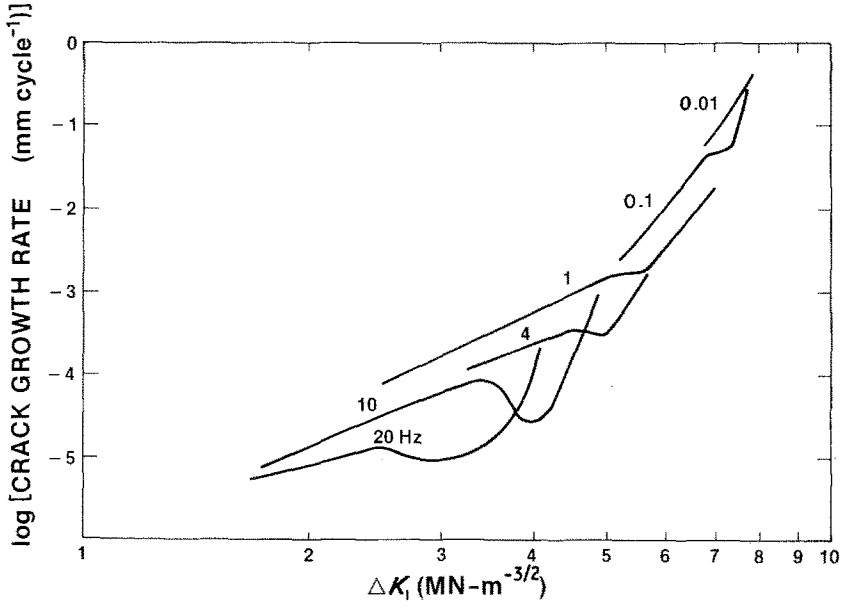

Figure 2 FCP data (smoothed) for 0.01 to 20 Hz.

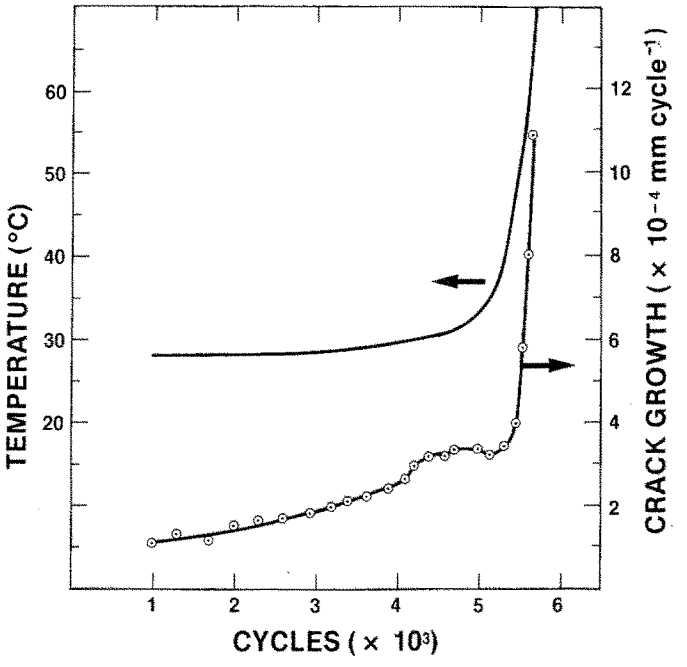

Figure 3 FCP and surface temperature for a 4 Hz test showing the rapid temperature rise in the post-transition region.

of thermal runaway is delayed from $\Delta K_I = 4\,MN\,m^{-3/2}$ to nearly double that value.

The pre-transition zone, however, shows only a slight frequency dependence over nearly five decades of crack growth rates. Where the data at different frequencies overlap (in ΔK_I range), there appears to be a small increase in rates with lower frequency, which may reflect a creep contribution.

Additional FCP tests were performed under square wave loading for frequencies of 0.1 and 1.0 Hz. The load rise time was 20 msec with an overshoot of approximately 5 to 10%. The FCP results are shown in Fig. 5, which compares the square wave results with the sine wave results at the same frequencies. At 1 Hz the square wave data exhibit a thermal transition at $\Delta K_I^* = 3.5\,MN\,m^{-3/2}$ compared to $\Delta K_I^* = 5.2$ for the sine wave loading. At 0.1 Hz the corresponding values are 5.1 and 6.8 $MN\,m^{-3/2}$, respectively. These results indicate the greater hysteretic

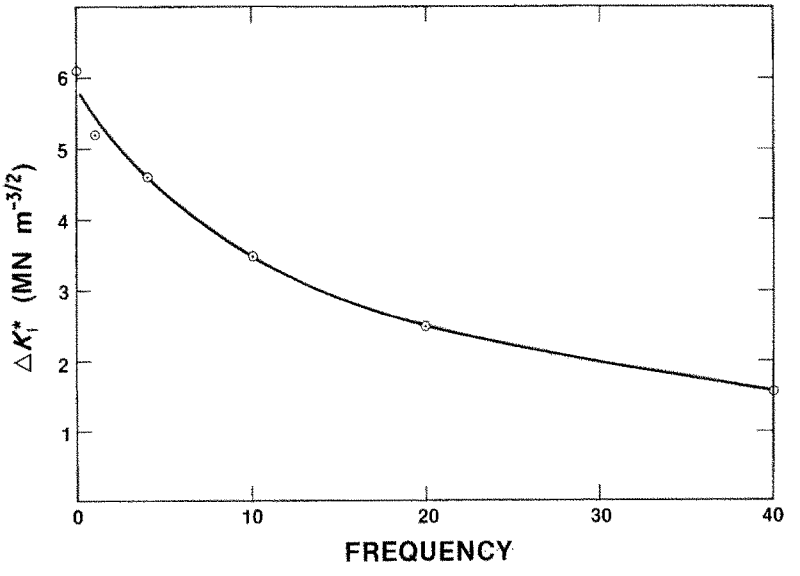

Figure 4 The onset of the thermal transition (ΔK_I^*) plotted against test frequency.

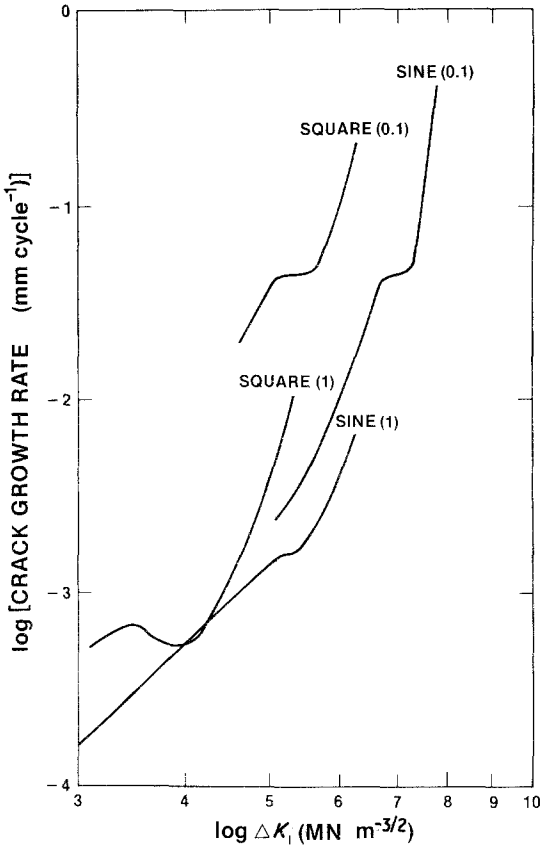

Figure 5 Waveform dependency of FCP. Square and sine wave results (smoothed) at 0.1 and 1.0 Hz.

heating for the fast loading rates in the square wave loading.

At both frequencies the square wave test results show enhanced crack growth rates over those for the sine wave loading. For the 1 Hz tests the square wave pre-transition growth rates exceed the sine wave results by a factor of 2 or 3 at comparable ΔK_I values, while the 0.1 Hz square wave results exceed the 0.1 Hz sine wave results by more than an order of magnitude. These more rapid growth rates probably reflect a creep contribution which should be more important in the square wave loading.

5. Pre-transition: secondary craze fracture

The pre-transition region is characterized by a macroscopically smooth fracture surface with no specimen width contractions (Fig. 6). At higher magnifications scanning electron micrographs reveal many polygonal surface features which are flat in the interior with raised perimeters, similar to lunar craters (Fig. 7). Small dimples are sometimes seen within the craters on the side closer to

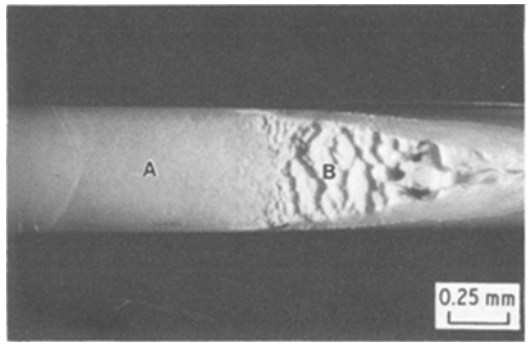

Figure 6 Typical fatigue fracture surface at 10 Hz. The crack growth is from left to right. The pre-transition region (A) is macroscopically smooth, whereas the transition and post-transition regions (B) are rough in the interior with thickening shear lips.

the direction from which the crack grew. They appear to be the nucleation sites of these fracture surface features. Similar surface structures have been seen in the fast fracture of PBT [23] and in FCP tests of semicrystalline polymers [1], where they have been described as voids and the mechanism of merger of several of these voids as void coalescence. Each crater was believed to represent a single void which nucleated and grew ahead of the crack tip. The crack propagation was thus viewed as the successive advance of the crack front through adjacent preceeding voids. It has been suggested that these voids may sometimes be crazes [1], thus the process of void coalescence would then be one of craze merger.

Our observations (especially the subsurface studies to be presented shortly) strongly suggest that PBT fatigue cracks are indeed preceeded by secondary crazes. The appearance of craze nuclei dimples and the somewhat parabolic shape of the perimeter of some of the craters (with the foci facing the crack front direction) indicate that the crazes fractured first, then merged with the advancing primary crack. It thus appears that the process of crack advance in PBT in the pre-transition region is one of secondary fracture of preceding crazes.

Secondary cracking has been well known to produce parabolic (or hyperbolic) fracture surface markings in amorphous polymers (see, for example, [24]) and the crater-like structures are most likely the semicrystalline analogue of the parabolic markings. The flat interior corresponds to the fractured craze plane and the sloped rim where two adjacent

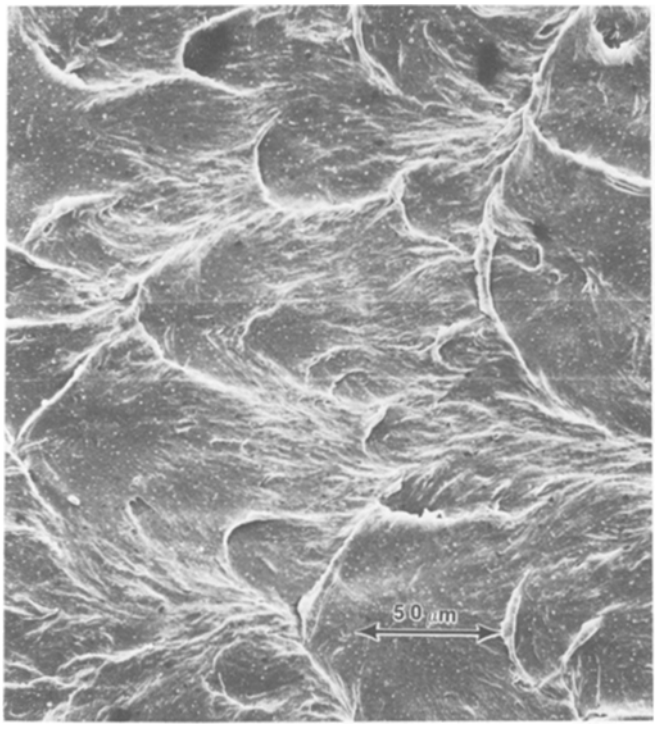

Figure 7 Crater-like frequency surface formations which suggest secondary fracture of preceeding crazes. The crack growth is from left to right. The foci are probably the nucleation site for these crazes.

crazes (not necessarily in the same plane) meet and local ductile shear flow (tearing) occurs.

Additional crazing occurs in the subsurface damage zone on either side of the crack plane, as shown in Fig. 8. The crack plane is very flat (normal to loading direction) in this pre-transition region with several layers of subsurface crazes diverging from the craze plane at angles between 10 and 20° C. These crazes appear to have initiated in the high stress region near the crack tip. As the crack tip propagated through the forward craze the existing subsurface crazes grew away from the plane as new crazes initiated near the new crack front. A cross-sectional view (plane normal to the

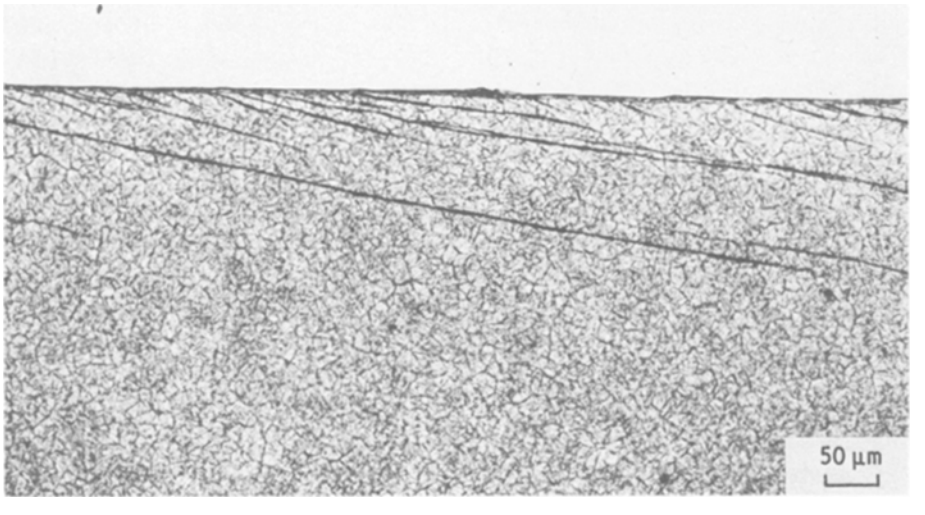

Figure 8 Subsurface view showing multiple crazes in the crack layer (transmission optical micrograph). The crack growth is from left to right.

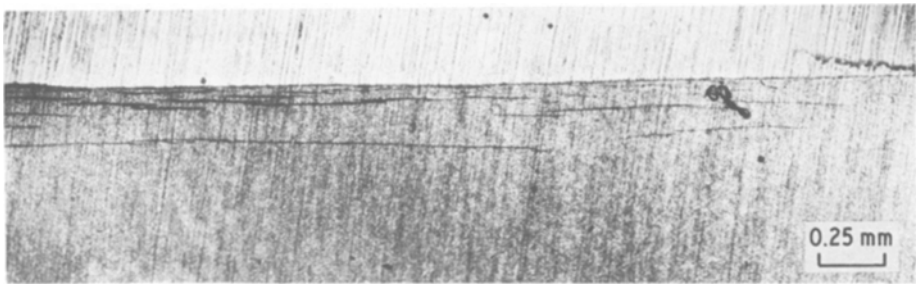

Figure 9 Cross-sectional view showing the craze layers (transmission optical micrograph). The crack growth is into the plane of the micrograph.

crack growth direction) would thus intersect the fracture surface as well as several layers of subsurface crazes, with the older crazes generally being further away from the crack plane (Fig. 9). Very similar fatigue crack advance mechanisms have been seen in an amorphous polymer blend of poly(2,6-dimethyl-1,4-phenylene oxide) and polystyrene [4].

6. Transition and post-transition

At the thermal transition the macroscopically smooth fracture surface becomes rough in the central region with shear lips forming on either side (Fig. 6). Considerable specimen width contraction and shear lip thickening can be seen along the crack growth direction. These features are more dramatic for the high frequency tests. The lower frequency (< 1 Hz) test specimens exhibit a more gradual transition from a macroscopically smooth region with small crater-like features to a slightly rougher region with larger craters.

At the onset of the transition, as denoted by the deceleration in the FCP data, the shear lips are very small and they remain relatively small until the crack is well into the thermal runaway portion of the FCP curve. During thermal runaway the hysteretic heating causes a rapid drop in the yield stress (σ_y) as an increase in the crack tip plastic zone size (R_p) (since $R_p \sim \sigma_y^{-2}$). The shear lips, which reflect the plane stress yield zone near the specimen free surfaces, thus thicken rapidly.

Cross-sectional subsurface views of the fatigue fracture process in this post-transition region reveal extensive crazing in the central regions and craze-free shear zones at both free surfaces (Fig. 10). The craze damage zone is deep and has a high density of crazes, leading to extensive stress-whitening. The crazes terminate abruptly near the free surface shear zones. The fracture surface profile is no longer flat, but shows large peaks and valleys consistent with the fracture surface observations (Fig. 6).

The craze damage zone is composed of long crazes which emanate from the crack plane as well as smaller crazes which appear to initiate mainly in the interspherulitic boundaries (Fig. 11). These smaller crazes, many of which nucleate far from the crack tip grow along the interspherulitic boundaries or along radial lines through the spherulites in a direction roughly parallel to the longer crazes. This type of fatigue craze nucleation and growth has also been observed in polypropylene [25].

The rough fracture surface is caused by the undulatory path taken by the crack front. In this process, the crack intersects crazes in the damage

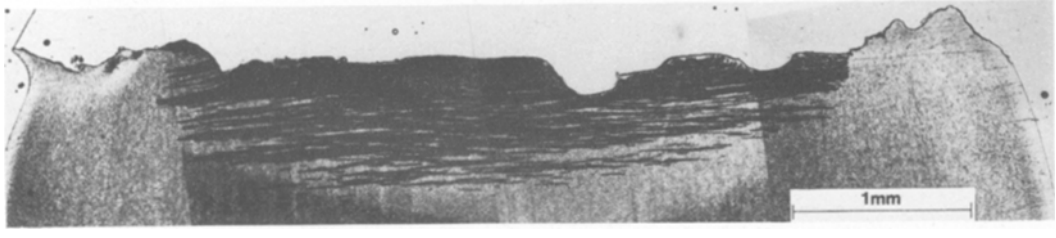

Figure 10 Cross-sectional view across the width of the sample during the post-transition region. The interior zone has a deep layer of crazes, which are flanked by sheared zones near the free surfaces. Note the roughness of the fracture surface profile in the interior region.

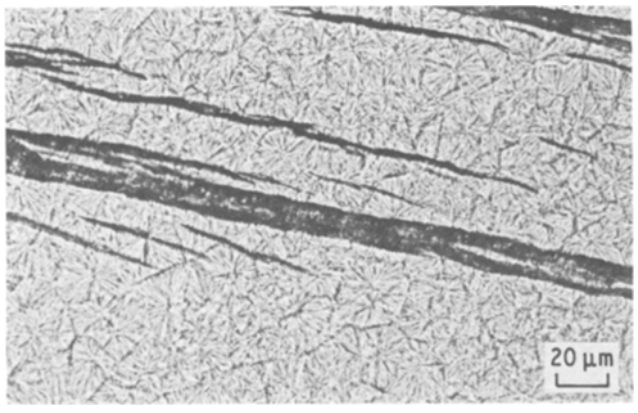

Figure 11 High magnification view deep in the craze layer showing small crazes nucleating at stress concentrations/weak sites in the spherulitic structure. The crack growth is from left to right.

zone. In Fig. 12 for example, bisected crazes can be seen with evidence of ductile drawing at the fracture surface (the bisected craze ends are turned upward). The truncated crazes appear as ridges on the sloped regions of the fracture surface (Fig. 13), similar to contour lines on a topographical map.

The shear zones show no stress whitening but considerable ductile tearing. The fracture surface shows a striated surface (Fig. 14) but these striations do not correspond to the individual load cycles until the very fast crack growth region near the final stages of crack growth. Near the free surfaces, the fracture surface appears rippled, much as a carpet that has been pushed together from both ends.

7. Immersion in water and silicone oil

Several samples were tested while they were immersed in distilled water or in medium viscosity General Electric silicone oil SF96(50). The increased thermal conductivity of the liquid media was expected to be more effective in reducing the heat accumulation near the crack tip. Although temperature measurements were not performed, greater heat dissipation was apparently achieved.

In Fig. 15, the results of three samples tested at 10 Hz are shown. The pronounced thermal transitions in the air-tested specimen is largely suppressed in the liquid-tested specimens. The crack growth rates appear to be slightly accelerated by water and silicone oil immersion in the pre-

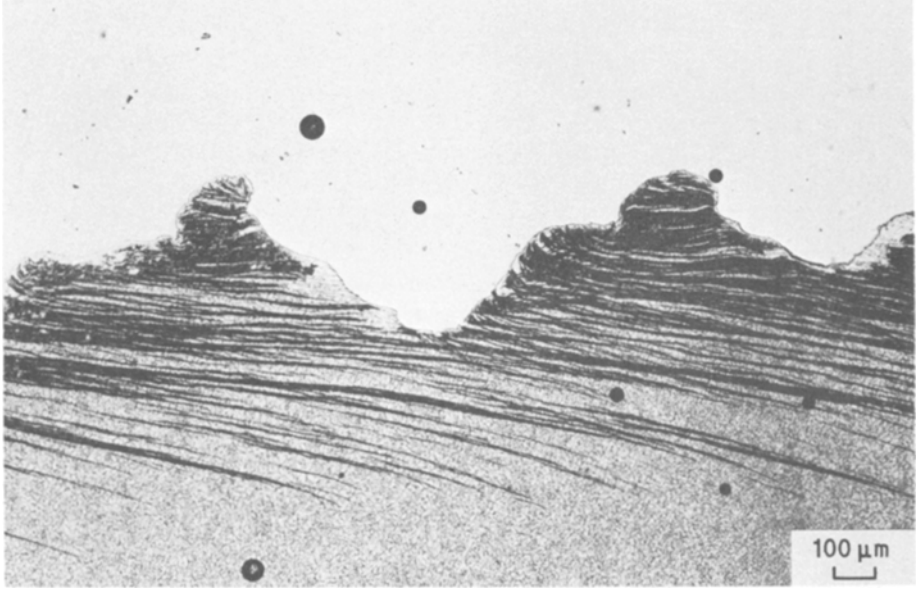

Figure 12 Subsurface view and the fracture surface profile in the post-transition region using transmission optical microscopy. Note the bisected crazes with turned up ends, indicating flow at the fracture surface. The crack growth is from left to right.

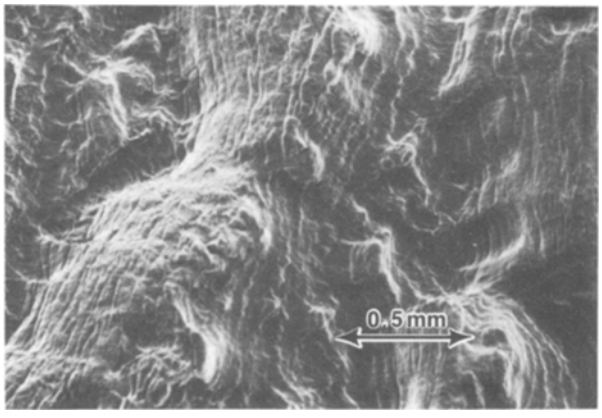

Figure 13 Fracture surface view (SEM) of a region similar to that in Fig. 12. The bisected craze ends appear as ridges, like contour lines in a topographical map. The crack growth is from left to right.

transition regions, but the thermal runaway is delayed to higher ΔK_I values.

The fracture surface vividly illustrates the effects of liquid immersion (Fig. 16). Both samples tested in the liquid media showed a delayed and much less dramatic change in the fracture surface topography, more reminiscent of the low frequency fracture surfaces. Furthermore, the rapid increase in shear lip development seen from the sample tested in air is not observed for the immersed samples.

The appearance of crater-like features on the fracture surface of the silicone oil immersed sample indicated that the fracture process was probably not significantly altered by the silicone oil immersion. For the water immersed samples, however, a dramatic change was observed. Although the fracture surface remained macroscopically smooth, the crater like features disappeared and were replaced with extensive shear drawing at the surface. Successive immersions into and removal from the water produced sharply demarcated fracture surface topographical features characteristic of each media (Fig. 17).

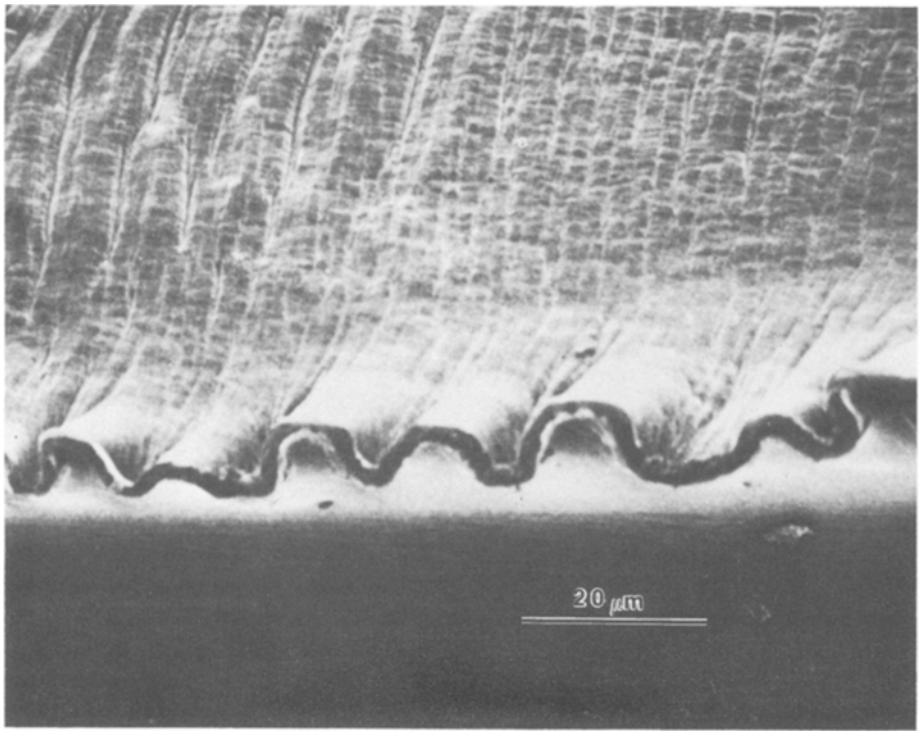

Figure 14 Fracture surface view (SEM) near the free surface, i.e. in the plane stress shear lip zones. The striations do not reflect single cycle advances. The crack growth is from left to right.

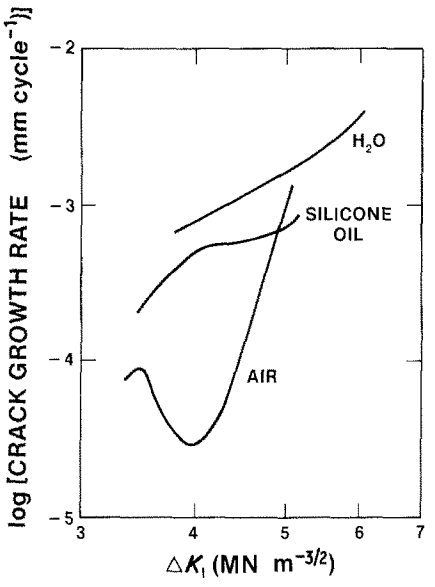

Figure 15 FCP results (smoothed) at 10 Hz for samples run in air and while submerged in water and silicone oil. Note the suppression of the thermal transition in the liquid immersed samples.

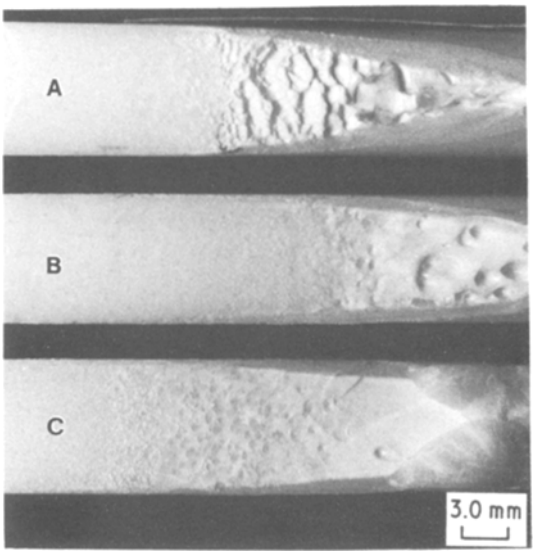

Figure 16 Comparison of the fracture surfaces (SEM) of samples tested at 10 Hz in air and while submerged in water or silicone oil.

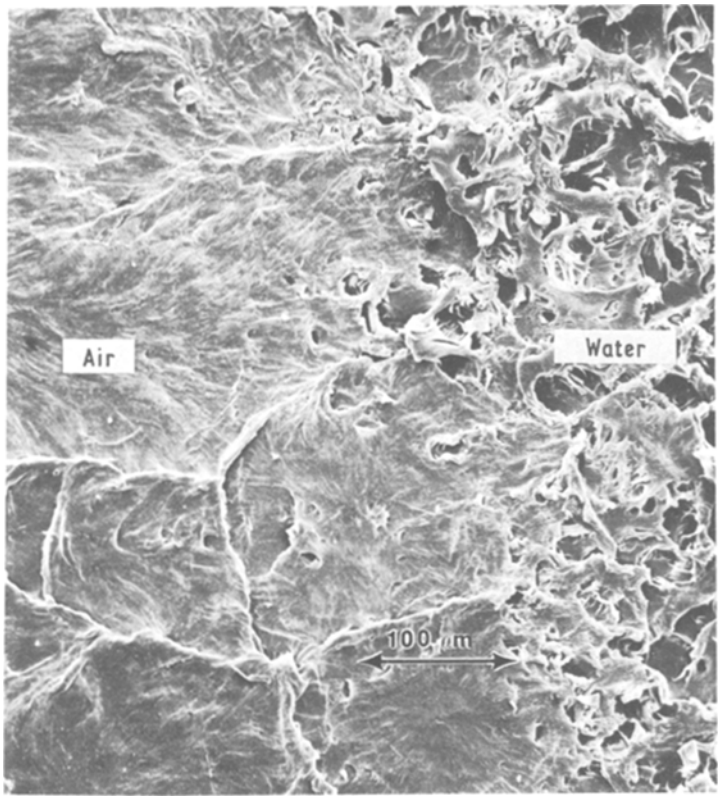

Figure 17 Fracture surface behaviour (SEM) in air and under water. Note the sharp demarcation between the two halves. The craters disappear and extensive shear drawing appears when the specimen is placed under water. Macroscopically, however, both surfaces appear smooth although their light-scattering behaviour is different, which makes visual identification possible.

During water immersion, a transition to the crater-like fracture surface was observed when the crack growth rate exceeded 10^{-3} mm per cycle. This strongly suggests a diffusion controlled process.

8. Summary and discussion

Since the test temperature is so close to the T_g of PBT ($\sim 50°$ C), hysteretic heating of the crack tip can lead to drastic changes in the surrounding bulk material. The drop in yield stress (at 80° C, it falls to less than one-half the 24° C value) produces a large increase in the depth of the crack tip damage layer. At the same time, the increase in the plane stress plastic zone near the free surfaces produces large shear lips which flank the interior craze zone. This crack layer transformation results in a crack growth rate transition, which appears as a crack deceleration followed by rapid crack acceleration. This transition is, of course, enhanced at the higher frequencies, where greater hysteretic heating can be expected.

The crack layer theory of FCP recently proposed by Chudnovsky and Moet [5] should be able to quantitatively describe this mode transition observed in PBT. According to this theory, the crack growth rate is given by:

$$\frac{dl}{dN} = \frac{\psi}{\gamma\omega - J_{1\max}} \qquad (1)$$

where ω is the crack layer width, γ the specific enthalpy of damage per unit ω, J_1 the energy release rate, and

$$\psi = \beta_0 \int_0^1 J_{1\max}(1)\, dl - Q \qquad (2)$$

where β_0 is the coefficient of energy dissipation, and Q the heat released.

Equation 1 has been used (with $Q = 0$) to describe the fatigue crack growth behaviour of polystyrene [26] and polypropylene [25]. In the latter case, a transition in the growth rate was shown to correlate with a shape change in the craze damage zone and with changes in the integrated areal craze density. With accurate measurements of Q and the kinetics of the damage development, the crack layer theory is similarly expected to accurately describe the mode transition in PBT.

Acknowledgement

The authors gratefully acknowledge the help of Jim Grande and Andy Holik with the optical microscopy.

References

1. P. E. BRETZ, R. W. HERTZBERG and J. A. MANSON, *Polymer* **22** (1981) 1272.
2. J. R. WHITE and J. W. TEH, *ibid.* **20** (1979) 764.
3. M. T. TAKEMORI and D. S. MATSUMOTO, *J. Polymer Sci. Polymer Phys. Ed.* **20** (1982) 2027.
4. T. A. MORELLI and M. T. TAKEMORI, *J. Mater. Sci.* **18** (1983) 1836.
5. A. CHUDNOVSKY and A. MOET, *Polymer Eng. Sci.* **22** (1982) 922.
6. M. N. RIDDELL, G. P. KOO and J. L. O'TOOLE, *ibid.* **6** (1966) 363.
7. G. P. KOO, M. N. RIDDELL and J. L. O'TOOLE, *ibid.* 7 (1967) 182.
8. K. WATKINSON, A. THOMAS and M. BEVIS, *J. Mater. Sci.* **17** (1982) 347.
9. Y. W. MAI, *J. Appl. Polymer Sci.* **26** (1981) 3947.
10. R. J. CRAWFORD and P. P. BENHAM, *Polymer* **16** (1975) 908.
11. *Idem, J. Mater. Sci.* 9 (1974) 18.
12. R. J. CRAWFORD, V. KLEWPATINOND and P. P. BENHAM, *Polymer* **20** (1979) 649.
13. R. J. CRAWFORD and P. P. BENHAM, *J. Mater. Sci.* 9 (1974) 1297.
14. R. W. HERTZBERG, M. D. SKIBO and J. A. MANSON, Fracture Mechanics: Twelfth Conference, ASTM STP 700, American Society for Testing and Materials (1979) p. 49.
15. A. SANDT and E. HORNBOGEN, *J. Mater. Sci.* **16** (1981) 2915.
16. E. H. ANDREWS and B. J. WALKER, *Proc. Roy. Soc. London A* **325** (1971) 57.
17. J. W. TEH, J. R. WHITE and E. H. ANDREWS, *Polymer* **20** (1979) 755.
18. P. E. BRETZ, R. W. HERTZBERG and J. A. MANSON, *ibid.* **22** (1981) 575.
19. *Idem, J. Mater. Sci.* **14** (1979) 2482.
20. R. W. HERTZBERG, M. D. SKIBO and J. A. MANSON, *ibid.* **13** (1978) 1038.
21. M. T. HAHN, R. W. HERTZBERG, J. A. MANSON, R. W. LANG and P. E. BRETZ, *Polymer* **23** (1982) 1675.
22. "1982 Annual Book of ASTM Standards", Part 10 (American Society for Testing and Materials, 1982) p. 765.
23. S. Y. HOBBS and C. F. PRATT, *J. Appl. Polymer Sci.* **19** (1975) 1701.
24. R. N. HOWARD, "The Physics of Glassy Polymers" (Wiley, New York, 1973) p. 388.
25. R. J. BANKERT, M. T. TAKEMORI, A. CHUDNOVSKY and A. MOET, *J. Appl. Phys.* (1983).
26. J. BOTSIS, A. MOET and A. CHUDNOVSKY, Society of Plastics Engineering, Inc., Technical Papers XXIX, SPE (1983) p. 444.

Received 7 April
and accepted 13 May 1983